Chemical Structures of Coprecipitated Fe−Ce Mixed Oxides

F. J. Pérez-Alonso, M. López Granados, M. Ojeda, P. Terreros, S. Rojas, T. Herranz, and J. L. G. Fierro*

Instituto de Catálisis y Petroleoquímica, CSIC, Marie Curie, 2, Cantoblanco, 28049 Madrid, Spain

M. Gracia and J. R. Gancedo

Instituto de Química-Física Rocasolano, CSIC, Serrano 119, 28006 Madrid, Spain

Received December 20, 2004. Revised Manuscript Received February 14, 2005

Two series of Fe−Ce catalysts were prepared following two different methods: coprecipitation from Fe and Ce nitrate solutions and physical mixing of pure Fe and Ce precursors. Evidence of the presence of a chemical interaction between Fe and Ce was found in the calcined state of the coprecipitated catalysts. Such evidence was obtained with different techniques. The Fe−Ce interaction occurs through the formation of hematite-like and cubic ceria-like solid solutions. In the hematite-like solid solution, Ce cations are dissolved in the hematite structure, whereas in the cubic ceria-like solid solution Fe cations are dissolved in the ceria structure. Such interactions were absent in the samples prepared by the physical mixing. It is suggested that the Fe−Ce interaction present in the calcined state results in a strong Fe−Ce interaction in the final catalyst that defines their better catalytic properties. When tested in the Fischer−Tropsch synthesis of hydrocarbons from $CO + H_2$ gas mixtures, the coprecipitation method series showed higher CO conversion rates, higher hydrocarbon formation rates, and a higher degree of olefinicity than the pure Fe catalyst sample and the Fe−Ce samples prepared by physical mixing.

1. Introduction

Ceria-based solutions with appropriate concentrations of oxygen vacancies and reduced cations (Ce^{3+}) are of great chemical and technological relevance because their properties and applications depend on the defect chemistry, and also on critical parameters of the dopant cation, such as ionic size and valence.[1] The oxygen vacancy concentration, and concomitant oxide ion conductivity, in cerium oxide can be increased by the substitution of a lower-valent metal ion (e.g., M^{3+}) for cerium. In the past, many investigations have been conducted on different aspects of ceria solid electrolyte, prepared mostly by conventional ceramic methods. However, the preparation temperature or time required to obtain a homogeneous solid solution depends to a significant extent on the particle size of the starting material. The host lattice of ceria is compatible with a range of rare-earth ion substitutions. Doped-ceria with trivalent ions (Pr^{3+} and Tb^{3+}) result in a lowering of the energy barrier for oxygen migration[2]; however, smaller homovalent ions (Zr^{4+}) enhance the oxygen storage capacity (OSC) by decreasing the activation energy for the reduction ($Ce^{4+} \rightarrow Ce^{3+}$) and retarding OSC degradation at high temperature. Given the effects that trivalent ions and smaller sizes have on the structure and properties,[3,4] there is considerable scientific interest in introducing M^{3+} ions into the ceria lattice.

Yttrium and samarium-doped ceria solid electrolytes have been prepared successfully by hydrothermal methods, providing low-temperature preparation and morphological control of ultrafine particles of uniform crystallite dimension.[5] Low-specific area ceria−zirconia solid solutions have been synthesized by several methods, such as high-temperature firing, high-energy milling of a mixture of the oxides, coprecipitation, combustion synthesis, and the sol−gel method.[6] Ultrafine particles of high-surface-area ceria−zirconia solid solutions and mesoporous ceria−zirconia solid solutions could be synthesized via a microemulsion method or a surfactant-assisted approach, respectively. However, for the crystallization of amorphous samples and/or the removal of the surfactants calcination is necessary.[7] This makes the preparation tedious and it may also generate pollutants from the oxidation/decomposition of the surfactants. Therefore, environmentally friendly synthesis of high-surface-area ceria−zirconia solid solutions is still a challenging issue.

Lower valence ions such as Fe^{3+} are extremely difficult to dissolve into the ceria lattice by conventional methods, since no solid solubility can be detected for Fe^{3+}-doped ceria sintered at 1473 K.[8] However, the synthesis of $Ce_{1-x}Fe_xO_2$ was achieved successfully under mild synthesis conditions according with a hydrothermal method. High-spin Fe^{3+} ions appeared to be distributed at Ce^{4+} and interstitial positions,

* To whom correspondence should be addressed. E-mail: jlgfierro@icp.csic.es.

(1) Murray, E. P.; Tsai, T.; Barnett, S. A. *Nature* **1999**, *400*, 649.
(2) Trovarelli, A. *Comments Inorg. Chem.* **1999**, *20*, 263.
(3) Balducci, G.; Kaspar, J.; Fornasiero, P.; Graziani, M.; Islam, M. S. *J. Phys. Chem. B* **1998** *102*, 557.
(4) Mamontov, E.; Egami, T.; Brezny, R.; Koranne, M.; Tiagi, S. *J. Phys. Chem. B* **2000**, *104*, 11110.
(5) Huang, W.; Shuk, P.; Greenblatt, M. *Chem. Mater.* **1997**, *9*, 2240.
(6) DeLeitenburg, C.; Trovarelli, A.; Zamar, F.; Maschio, N.; Dolcetti, G. G.; Llorca, J. *Chem. Commun.* **1995**, 2181.
(7) Masui, T.; Fujiwara, K.; Peng, Y.; Sakata, T.; Machida, K. I.; Mori, H.; Adachi, G. Y. *J. Alloys Compd.* **1998**, *269*, 116.
(8) Tianshu, Z.; Hing, P.; Huang H.; Kilner, J. *J. Mater. Proc. Technol.* **2001**, *113*, 463.

10.1021/cm0477669 CCC: $30.25
Published on Web 03/31/2005

accounting for the extremely low oxygen vacancy concentration and the absence of Ce^{3+}.[9] Within this framework, the research work presented here aims to shed some light on the effect of the addition of cerium on the structure of iron oxide systems. Accordingly, several iron−cerium oxides (with Ce/Fe atom ratios ranging from 0/1 to 0.5/0.5) were prepared by coprecipitation from Fe and Ce nitrate solutions. As demonstrated in the parent $Ce_{1-x}Mn_xO_2$ solid solution,[10,11] the coprecipitation methodology is expected to result in easy formation of Fe−Ce interactions in the final solid. A detailed structural characterization of pure Fe and Ce oxides and of the mixed oxide are reported. The properties of the coprecipitated Fe−Ce catalysts are compared with those of mixed Fe−Ce systems prepared by physical mixing of pure Fe and Ce phases with the same final Fe−Ce ratio as those coprecipitated.

Apart from the structural information deriving from the $Ce_{1-x}Fe_xO_2$ solid solution, the reactivity of exposed iron sites within and in close contact with this phase is also studied. Thus, the hydrogenation of CO was selected as a test reaction. Here we report for first time that oxides prepared by coprecipitation display better catalytic conversion than those prepared by physical mixing. In other words, catalysts in which an Fe−O−Ce interaction is developed in the oxide form exhibit better catalytic performance.

2. Experimental

2.1 Catalyst Preparation. A series of coprecipitated iron−cerium catalysts with 100, 95, 85, 50, and 0 at. % Fe metal (Ce balance) was prepared by batchwise coprecipitation under vigorous stirring from 1 M aqueous solutions of $Fe(NO_3)_3{\cdot}9H_2O$ (Fluka puriss. p.a. ACS: 98−101%) and $Ce(NO_3)_3{\cdot}6H_2O$ (Aldrich 99.99%), with a 5.6 M NH_4OH solution. Both solutions were simultaneously added at a constant rate of 50 mL/h by a perfusion pump (Becton Dickinson SE 400) to a precipitating batch containing 500 mL of distilled water at the start. Addition of the precipitating agent (NH_4OH) was accomplished using a pH-stationary device (Radiometer Copenhagen; ABU91 Autoburet), maintaining the pH constant (at 8.0) during precipitation. Temperature was kept at 343 K. The precipitate thus obtained was aged for 16 h with the mother liquors still under stirring at the reaction temperature, maintaining pH at 8. Then, the precipitate was filtered out and washed with successive portions of 400 mL of distilled water at 323 K. The precipitates were dried in air at 333 K for 24 h and called precursors. Catalysts were obtained by calcination under ambient air at 573 K for 6 h (unless otherwise stated). These solids were referred to as 100Fe (pure Fe), 95Fe, 85Fe, 50Fe, and Ce (pure Ce). For samples calcined at higher temperatures, the end of the label indicates the *T* at which it was calcined, e.g., 50Fec773 means that the precursor was now calcined at 773 K (instead of at 573 K).

Another series of catalyst was prepared by physically mixing the pure Fe and Ce precursors. The pure Fe and pure Ce precursors (dried precipitates) described in the previous paragraph were used for the preparation of the physical mixtures. The pure precipitates were mixed at the ratio required to obtain two different mixed Fe−Ce precursors: 85 and 50 at. % of Fe, respectively (TGA analysis of the 100Fe and Ce was used to estimate the mixing ratios). The samples were finely ground before calcining under ambient air at 573 K for 6 h and are referred to as PM85Fe and PM50Fe.

2.2 Characterization Techniques. Powder X-ray diffraction (XRD) patterns were recorded in the 5−80° 2θ range in scan mode (0.02°, 2 s) using a Seifert 3000 XRD diffractometer equipped with a PW goniometer with Bragg−Brentano $\theta/2\theta$ geometry, an automatic slit, and a bent graphite monochromator. In some cases, powdered Si was mixed with the samples and used as an internal standard. The unit cell parameters were obtained by refining the peak positions of the XRD patterns with a least squares refinement method using the CELREF program (CELREF unit-cell refinement software for Windows by Laugier and Bochu, http://www.ccp14.ac.uk/). To determine peak positions, the peak profiles were fitted with the commercially available ANALYZE program (pseudo-Voigt function).

Raman spectra were recorded with a Renishaw 1000 spectrophotometer equipped with a cooled CCD detector (200 K) and a holographic Notch filter that removes the elastic scattering. The samples were excited with the 514-nm Ar line. Acquisition of spectra consisted of 5 accumulations of 60 s. All samples were pretreated in situ in 100 mL/min (STP) of air at 523 K for 30 min before recording the spectra in an in situ cell (Linkam, TS-1500). The spectra were collected at 473 K under an air flow.

Nitrogen adsorption isotherms were recorded at the temperature of liquid nitrogen (77 K), using a Micromeritics ASAP 2000 apparatus. Samples were degassed at 413 K for 12 h prior to the determination of the adsorption isotherm.

Transmission ^{57}Fe-Mössbauer spectra were recorded at room temperature (RT) from precursor and catalyst samples using a conventional constant-acceleration spectrometer equipped with a ^{57}Co (Rh) source. RT absorbers were prepared to provide an effective thickness of about 10 mg cm^{-2} of natural Fe. Low-temperature spectra were recorded at several temperatures between 10 and 100 K from samples 95Fe, 85Fe, and 50Fe, using a closed-cycle He cryogenerator (Air Products Inc.). The low-temperature absorber was prepared by sandwiching a mixture of powdered sample and vacuum grease between two pieces of aluminum foil. The spectra were computer-fitted by two different procedures. The first was a fitting to a sum of Lorentzian lines by applying the constraints of equal line width and area for the two peaks of doublets, and equal line width and areas at a ratio of 3:2:1:1:2:3 for the six peaks of sextets. A second procedure based on hyperfine magnetic field (H) distributions was used to fit some of the low-temperature spectra. When using this procedure, a Lorentzian shape for the lines and no predetermined pattern for distribution were assumed, affording histograms of H probabilities. Isomer shifts were referred to the center of the α-Fe sextet at RT. The relative concentrations of the different Fe species were calculated from their spectral area ratios, assuming equal *f* factors (probability of a Mössbauer effect) for all the Fe species present in the spectrum.

2.3 Catalytic Measurements. The catalysts were tested in the CO hydrogenation reaction using a fixed-bed microreactor (stainless steel 316, 150 mm long and 9 mm i.d.). The reactor temperature was measured with a K-type thermocouple buried in the catalytic bed. Flow rates were controlled using a Brooks 5850 TR Series mass flow controller.

The calcined samples (200 mg, 0.25−0.30-mm particle size) were diluted with SiC (ca. 2 g, 0.25−0.30-mm particle size) to avoid hot spots. First, the catalysts were activated in situ at 673 K (heating rate of 10 K/min) for 16 h in hydrogen (5.9 NL (H_2)/min), H_2/N_2(1:2) at atmospheric pressure. The reactor was then cooled to the reaction temperature (573 K) and the system was pressurized to 1.01 MPa, both processes using an inert gas (N_2). After the system had been pressurized, the flow was switched to synthesis

(9) Li. G.; Smith, R. I.; Inomata, H. *J. Am. Chem. Soc.* **2001**, *123*, 11091.
(10) Machida, M.; Uto, M.; Kurogi, D.; Kijima, T. *Chem. Mater.* **2000**, *12*, 3158.
(11) Machida, M.; Kurogi, D.; Kijima, T. *Chem. Mater.* **2000**, *12*, 3165.

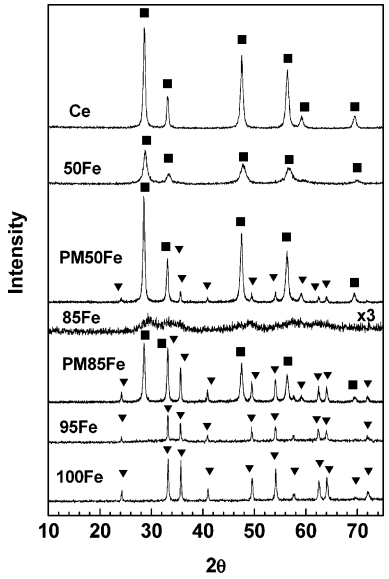

Figure 1. XRD patterns of the samples calcined at 573 K: (■) *c*-CeO_2; (▼) α-Fe_2O_3.

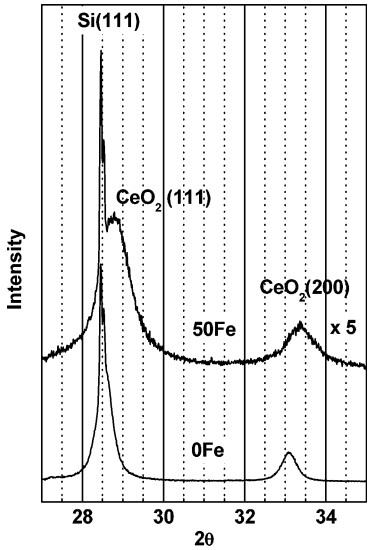

Figure 2. XRD patterns of a mixture of 0Fe and 50Fe samples calcined at 573 K and Si ($2\theta = 27-35°$): *c*-CeO_2; α-Fe_2O_3.

gas ($H_2/CO = 2$; GHSV = 0.0043 $Lg^{-1}s^{-1}$). This moment was considered as the initial time of the reaction. It was estimated that at this pressure and with this flow rate the reaction mixture would have flushed the N_2 in 45−50 min.

Product analysis was performed on-line with a gas chromatograph (HP 6890 Plus) equipped with a cryogenic unit that allowed the GC oven to be cooled to 223 K. A Porapak Q ($^1/_8$ in. × 3 m)-packed column connected to a thermal conductivity detector was used to analyze the inorganic gases (H_2, N_2, CO, CO_2) and water. Hydrocarbons and oxygenated compounds were analyzed in a DB-1 capillary column (60 m × 0.25 mm × 0.25 μm) connected to a flame ionization detector. The following temperature program was used: 223 K for 10 min, then a ramp of 10 K/min to 523 K, and then keep at this temperature for 20 min. N_2 was used as internal standard for chromatographic analyses.

Results

Figure 1 shows the diffractograms of the catalyst (calcined precursors at 573 K) samples. The reflections observed in the figure can be assigned either to hematite, α-Fe_2O_3, (hexagonal, $R\bar{3}c$)[12] or cubic CeO_2 (fluorite structure, $Fm3m$).[13] In the case of 100Fe, only α-Fe_2O_3 reflections (marked as ▼) whereas those of *c*-CeO_2 (■) in the case of Ce sample. Physically mixed samples (PM50Fe and PM85Fe) displayed reflections from both phases. In the samples prepared by coprecipitation, the situation was not as simple. The 95Fe sample displayed reflections only from α-Fe_2O_3 but not from Ce oxide. At the other end of the composition range, the 50Fe sample, only reflections arising from *c*-CeO_2 were visible. In addition, they were wider than those arising from the *c*-CeO_2 detected in the Ce sample and in the PM50Fe or PM85Fe samples. The wider reflections indicate that the phases displayed smaller crystal size and/or microstrain (mainly variations in the lattice parameters due to the inhomogeneity of the composition of the phases formed during coprecipitation).[14] In the case of the 85Fe sample, the low intensity of the reflections observed indicates poor crystallization of the sample. This hinders the straightforward assignment of the reflections to a particular phase but it seems that either α-Fe_2O_3[12] or *c*-CeO_2, both with very small crystal size, would be present.

Figure 2 represents a selected region of the diffractograms of the Ce sample (pure CeO_2) and of the coprecipitated sample 50Fe. For correct assignation of the peaks, Si powder was used as an internal standard. The (111) reflection of the Si powder (both $K\alpha_I$ and $K\alpha_{II}$ reflections are visible) and the (111) and (200) reflections of the CeO_2 structure were observed. In the case of the pure CeO_2 sample (Ce), the (111) reflection of the ceria was superimposed and seen as a shoulder of the Si (111) reflection. However, in the co-precipitated sample the CeO_2 (111) peak shifts toward higher diffraction angles. This shift is more evident when (200) reflections are compared, and this indicates that a mixed Ce−Fe oxide (very likely present as a solid solution) is formed, its structure corresponding to that of the *c*-CeO_2 in which some of the Ce^{4+} cations have been substituted by Fe^{3+} cations. The mixed oxide can tentatively be formulated as $Ce_{0.5}Fe_{0.5}O_{2-\delta}$, indicating that electrical neutrality is achieved by the O-vacancy formation mechanism. The substitution originates a contraction of the unit cell because of the smaller size of the Fe^{3+} cation (0.64 Å) as compared to that of the Ce^{4+} cation (1.01 Å).[13] This contraction was evident from the unit cell parameter: 5.4170 Å for the Ce sample vs 5.3716 Å for the 50Fe sample (see Table 1). In the case of the 95Fe sample, a shift to lower Bragg angles of the α-Fe_2O_3 reflections was observed and its *a* and *c* parameters were larger than those of the 100Fe sample: 5.0454 and 13.7833 Å vs 5.0368 and 13.7601 Å, respectively (see Table 1). This can be ascribed to the formation of a mixed oxide (very likely present as a solid solution) with the α-Fe_2O_3 structure in which Fe^{3+} cations have been substituted by the larger Ce^{4+}

(12) Cornell, R. M.; Schwertmann, U. *The Iron Oxides: Structure, Properties, Reactions and Uses*; VCH Publishers: New York, 1996.
(13) Kăspar, J., Fornasiero, P., Eds.; *Catalysis by Ceria and Related Materials*; Imperial College Press: London, 2002.
(14) Kimmel, G.; Dayan, D. In *IUCR Monographs on Crystallography*; Snyder, R. L., Fiala, J., Bunge, H. J., Eds.; Oxford Science Publications: Oxford, U.K., 1999; N*o*. 10, pp 698−727.

Table 1. Unit Cell Parameters of the Phases Detected in the Different Samples as Determined by CELREF

	CeO_2				α-Fe_2O_3			
	Ce	50Fe	PM85Fe	PM50Fe	100Fe	95Fe	PM85Fe	PM50Fe
a (Å)	5.4170 ± 0.0012	5.3716 ± 0.0134	5.4172 ± 0.0055	5.4194 ± 0.043	5.0368 ± 0.0015	5.0454 ± 0.0006	5.0364 ± 0.0013	5.0366 ± 0.0013
c (Å)					13.7601 ± 0.0003	13.7833 ± 0.0001	13.7686 ± 0.0004	13.7692 ± 0.0004

Results for Samples Calcined at 973 K

	CeO_2		α-Fe_2O_3		
	50Fec973	85Fec973	95Fec973	85Fec973	50Fec973
a (Å)	5.4062 ± 0.0018	5.3773 ± 0.0086	5.0388 ± 0.0003	5.0376 ± 0.0006	5.0406 ± 0.0008
c (Å)			13.7590 ± 0.0040	13.7630 ± 0.0090	13.7596 ± 0.0012

cations. The electrical neutrality of the solid can be achieved either by an excess of O^{2-} anions (in this case the solid solution is described by the stoichiometric formula: $Fe_{1.95}Ce_{0.05}O_{3+\delta}$) or by the presence of OH groups instead of O^{2-} ($Fe_{1.95}Ce_{0.05}O_3OH_x$).[12] A similar effect has also been reported for other Fe−Ce systems prepared by coprecipitation[15] and by the citrate method.[16] Concerning the nature of the samples prepared by physical mixing (PM85Fe and PM50Fe), and according to the data summarized in Table 1, the cell constant parameters determined from the *c*-CeO_2 and α-Fe_2O_3 reflections are very close to those of pure phases. This indicates that solid solutions are not formed.

Figure 3 shows the XRD spectra of the samples obtained after calcination of the 50Fe precursor at three different temperatures: 573, 773, and 973 K. As discussed above, the sample calcined at 573 K showed the diffraction peaks of the *c*-CeO_2 (■) shifted to higher Bragg angles due to the formation of an Fe−Ce mixed oxide. After calcination at 773 K, the reflections from *c*-CeO_2 (■) and those of an incipient α-Fe_2O_3 (▼) were also visible. The values of the cell parameter of *c*-CeO_2, *a*, and of the full width at medium height of the reflections are similar to those of the 50Fe sample, indicating that most of the mixed oxide still remains unaltered. However calcination at higher temperatures (50Fec973) resulted in important changes in the reflections: the peaks from α-Fe_2O_3 and from *c*-CeO_2 were narrower, indicating a better crystallization of those phases. Moreover, the unit cell parameter deduced from the reflections of *c*-CeO_2 moved to 5.4062 (± 0.0018), higher than that of the 50Fe sample (see Table 1) and fairly similar to that of the pure Ce sample. It is clear that calcination at higher temperatures may result in the formation of pure α-Fe_2O_3 and *c*-CeO_2 phases from the Fe−Ce mixed oxide. This is confirmed by the results shown in Figure 4, where the XRD patterns of 95Fec973 and 85Fec973 are offered (for comparative purposes, 50Fec973 is also shown). For the 95Fec973 sample, it can be seen that calcination at 973 K results in the narrowing of the α-Fe_2O_3 peaks with respect to those of the 95Fe sample, while incipient *c*-CeO_2-like reflections were observed. Moreover, the shift of the *a* and *c* of the α-Fe_2O_3 parameters toward those of pure hematite should be noted (see Table 1). That of the *c*-CeO_2 solid solution could not be determined accurately. In the case of the 85Fec973 sample, although the situation is slightly different the hypothesis that calcination at high-temperature results in the formation of pure phases from mixed oxides is still supported. The hematite reflections corresponded to those of pure α-Fe_2O_3: its lattice parameters were 5.0376 and 13.7630 Å, similar to those of the 100Fe sample. However, the lattice parameter deduced from ceria reflections (5.3773 Å) indicated that part of the Fe^{3+} was still inside the *c*-CeO_2 structure and that segregation into two pure phases had not been fully achieved. It is worth stressing that in the sample calcined at 573 K (85Fe) no crystalline phases were detected

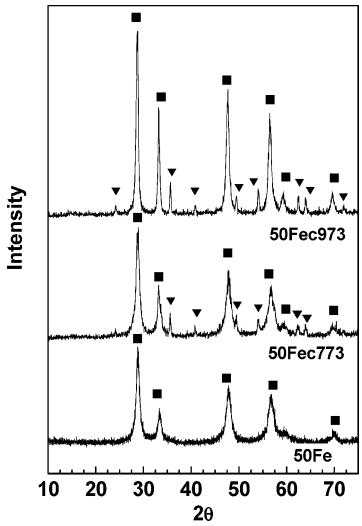

Figure 3. XRD patterns of the 50Fe calcined at different temperatures: (■) *c*-CeO_2; (▼) α-Fe_2O_3.

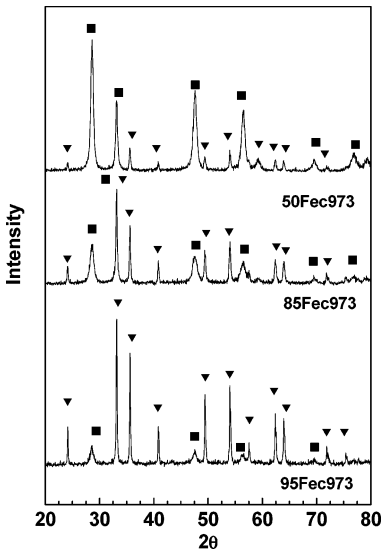

Figure 4. XRD patterns of the 50Fe, 85Fe, and 95 Fe samples calcined at 973 K: (■) *c*-CeO_2; (▼) α-Fe_2O_3.

(15) Neri, G.; Pistone, A.; Milone, C.; Galvagno, S. *Appl. Catal. B: Environ.* **2002**, *38*, 321.
(16) Kamimura, Y.; Sato, S.; Takahashi, R.; Sodesawa, T.; Akashi, T. *Appl. Catal. A: Gen.* **2003**, *252*, 399.

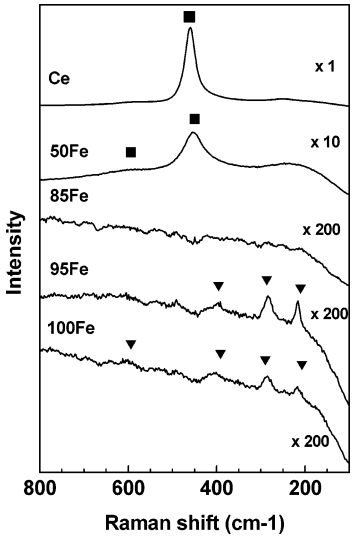

Figure 5. Raman spectra of the 0Fe, 50Fe, 85Fe, 95 Fe, and 100Fe samples calcined at 573 K: (■) *c*-CeO_2; (▼) α-Fe_2O_3.

and therefore calcination at 973 K is required for the detection of these phases.

The Raman spectra for calcined samples are shown in Figure 5. The Raman spectrum of the Ce sample corresponds to the well-documented Raman spectrum for *c*-CeO_2;[17] an intense band at 460 cm^{-1} that has been assigned to a symmetric breathing mode of the O-atoms around each Ce^{4+} cation (metal dioxides with a fluorite structure have only a single allowed Raman mode with F_{2g} symmetry). The features observed in the spectrum of the pure Fe catalyst (100Fe) correspond to that of α-Fe_2O_3.[18] In the region shown in the figure, seven lines were expected (two A_{1g} modes and five E_g modes) but only four phonons were detected: 218, 286, 404, and 604 cm^{-1}. The peak located at ca. 290 cm^{-1} is a doublet, difficult to solve in most of the Raman spectra reported: a very low temperature (100 K) is needed to solve them.[18] The weak peaks at ca. 240 and 495 cm^{-1}, which are visible in very crystalline α-Fe_2O_3, are missing due to the lower crystallite size of the Fe oxides prepared by precipitation.[19] The lower intensity of the features of 100Fe sample with respect to that of Ce sample must be related to the fact that Fe oxides absorb laser light (and scattered Raman radiation) due to the strong absorbance of hematite at the wavenumber region of the Raman spectrum.[12] This results in a decrease in the sampling depth where the Raman line arises from and, consequently, in a loss of the intensity of the Raman bands.[20]

The spectrum of the 95Fe sample is similar to that of the 100Fe sample: hematite features were visible, whereas those from *c*-CeO_2 were undetectable. This is in keeping with the XRD results, which only showed α-Fe_2O_3-like reflections. In the case of the 85Fe catalyst, neither CeO_2 nor Fe_2O_3 bands could be observed clearly. Very broad features were observed by XRD (in all probability due to the very small size of the crystallites of the oxides, which could also be the reason for the absence of Raman features[18,21]).

In the case of the 50Fe catalyst, although the Raman spectrum for the mixed oxide 50Fe resembled that of pure CeO_2, several features should be highlighted. First, the main Raman band shifted to lower frequency (451 cm^{-1}) with respect to that of pure *c*-CeO_2 (460 cm^{-1}). It also broadened and developed a low-frequency tail. The tail can be associated with smaller crystal size[22,23] of the oxide since it was detected in the XRD results. The shift to lower frequency of the main Raman peak is the final result of two opposite effects: the contraction of the unit cell due to the formation of the mixed oxide, resulting in a shift to higher frequency,[17] and the decrease in the crystal particle size, resulting in the opposite shift and finally predominating.[23]

In this sample, it is worth noting the weak band at ca. 590 cm^{-1} because this is relevant for the detection of O vacancies. In $Ce_{1-x}M_xO_{2-\delta}$ mixed oxides (M: trivalent metal) this feature has been assigned to the presence of O-vacancies. These vacancies are associated with the Ce^{4+} substitution by the trivalent M^{3+} and are created because of the vacancy compensation mechanism.[17] The strong Ce^{4+} substitution by Fe^{3+} cations (ca. 50%) should have resulted in a remarkable number of O vacancies, and therefore in a very intense Raman band if the charge balance had been achieved by the vacancy compensation.[13] This was not the case in the Raman spectrum of the 50Fe sample. A plausible explanation is that a mechanism other than Ce^{4+} substitution could take place instead. This would be the so-called dopant interstitial compensation mechanism,[13] in which three Ce^{4+} are substituted by three Fe^{3+} cations and neutrality is accomplished by the location of one additional Fe^{3+} cation in the interstitial sites of the fluorite *c*-CeO_2 structure. In fact, calculations based on atomistic simulations have shown that although the vacancy compensation mechanism is energetically favored in the solid solutions formed between trivalent cations and CeO_2, the cation compensation mechanism is not so much favored for the smallest trivalent cations such as Ga^{3+}, Cr^{3+}, Al^{3+}, or Fe^{3+} as compared to the dopant interstitial mechanism.[24] And the latter mechanism has been also claimed by Li et al. to occur in Ce-rich Fe−Ce−O mixed oxides.[9] In sum, the δ value in the tentative stoichiometric formula of the solid solution ($Ce_{0.5}Fe_{0.5}O_{2-\delta}$) is close to zero and this is why the band at ca. 570 cm^{-1} is very weak; the dopant interstitial mechanism seems to be the predominant option to accommodate Fe^{3+} cations in the *c*-CeO_2 structure. The Raman spectra of the samples after calcination at 973 K (not shown in this work) agree with the conclusions derived from the XRD results: segregation of the pure oxides from the solid solutions.

Figure 6 represents the specific surface areas of the samples as determined by the BET method. It is clear that the preparation of Fe−Ce oxides by coprecipitation resulted in samples with higher specific areas than the pure Fe or Ce

(17) McBride, J. R.; Hass, K. C.; Poindexter, B. D.; Weber, W. H. *J. Appl. Phys.* **1994**, *76*, 2435.
(18) De Faria, D. L. A.; Silva, S. V.; De Oliveira, M. T. *J. Raman Spectrosc.* **1997**, *28*, 873.
(19) Magnacca, G. *Chem. Mater.* **2003**, *15*, 675.
(20) Xie, S. *J. Phys. Chem. B* **2003**, *105*, 5144.
(21) Zhang, F. *Appl. Phys. Lett.* **2002**, *80*, 127.
(22) Weber, W. H. *Phys. Rev. B* **1993**, *48*, 178.
(23) Spanier, J. E. *Phys. Rev. B* **2001**, 64, 245407.
(24) Minervini, L.; Zacate, M. O.; Grimes, R. W. *Solid State Ionics* **1999**, *116*, 339.

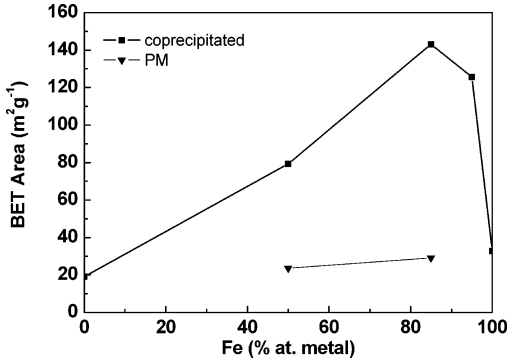

Figure 6. Specific surface areas determined by the BET method of samples calcined at 573 K.

Table 2. Mössbauer Parameters at Room Temperature[a]

	100Fe	95Fe	85Fe	50Fe	50Fec973	PM85Fe
			Sextet S_A			
δ (mm s^{-1})	0.38 (1)	0.38 (1)			0.38 (1)	0.38 (1)
2ϵ (mm s^{-1})	−0.22 (1)	−0.22 (1)			−0.22 (1)	−0.22 (1)
Γ (mm s^{-1})	0.37 (1)	0.36 (1)	>0.70		0.33 (1)	0.33 (1)
H (T)	51.47 (1)	51.47 (1)	≈50		51.55 (1)	51.49 (1)
A_{rel} (%)	100	50	≈5		86	100
			Doublet D			
δ (mm s^{-1})		0.34 (1)	0.34 (1)	0.34 (1)	0.32 (1)	
Δ (mm s^{-1})		0.79 (1)	0.80 (1)	0.81 (1)	0.99 (2)	
Γ (mm s^{-1})		0.54 (1)	0.56 (1)	0.58 (1)	0.81 (4)	
A_{rel} (%)		50	95	100	14	

[a] δ = isomer shift (relative to α−Fe); Δ = quadrupole splitting; 2ϵ = quadrupole shift; Γ = full line width at half-maximum; H = hyperfine magnetic field; A_{rel} = relative spectral area. Numbers in parentheses give the uncertainty in the last digit.

oxides. Nevertheless, it should be noted that a volcano-type dependency on the Ce-content was observed. A small addition of Ce during Fe precipitation (95Fe sample) resulted in a remarkable increase (4-fold) in the specific area. Further Ce addition (85Fe sample) further increased the specific surface area values. Beyond this point Ce addition seemed to produce samples with lower specific areas, though still larger than the pure Ce and Fe samples. It should also be stressed that the specific areas of the samples obtained by physical mixing appear to be the result of a linear combination of the areas of the pure phases.

A hyperfine magnetic sextet appears as the sole constituent in the RT Mössbauer spectra of 100Fe and PM85Fe samples, while only a paramagnetic doublet is present in the 50Fe spectrum. Sextets and doublet coexist in the other three spectra with a doublet/sextet area ratio increasing in the order of 50Fec973 < 95Fe < 85Fe. Thus, the presence of a doublet in the spectrum appears to be related to the Ce-content of the samples. The RT Mössbauer spectra were fitted by considering a hyperfine magnetic sextet (S_A) and/or a doublet (D) (see Figure 7). Table 2 shows the Mössbauer parameters obtained from the fits. The Mössbauer parameters of S_A are characteristic of hematite (α-Fe_2O_3).[25−27] The RT parameters of hematite are similar to those of the cerium orthoferrite ($CeFeO_3$),[28] it being difficult to differentiate both compounds

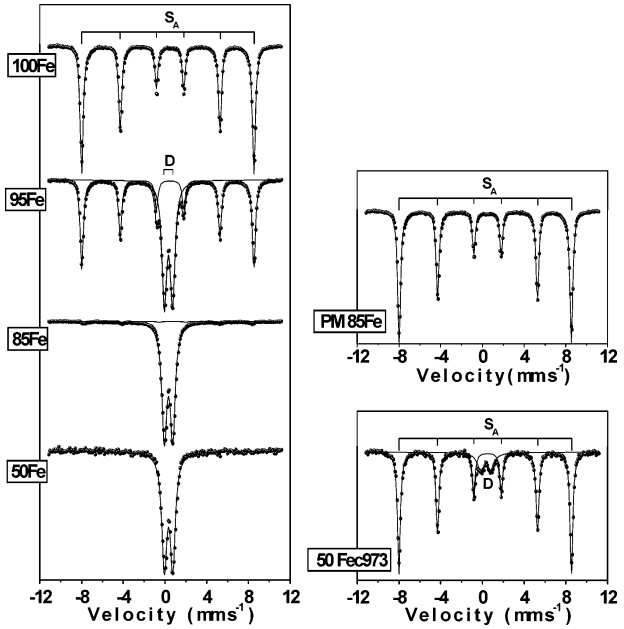

Figure 7. Mössbauer spectra recorded at RT from the four coprecipitated catalysts calcined at 573 K (left) and from catalysts PMFe85 and 50Fec973 (right). The computer fits are shown as solid lines.

from their corresponding Mössbauer data. Nevertheless, since the values obtained for the S_A parameters were practically identical in all the samples (see Table 2) and since the synthesis conditions and the XRD data (see above) rule out the existence of a significant concentration of $CeFeO_3$ in Ce-containing samples, it seems reasonable to attribute S_A to the hematite in all the samples. The parameters of D correspond to high-spin Fe^{3+} ions occupying distorted octahedral sites.[9] Amorphous or superparamagnetic (spm) iron oxides, poorly ordered hydrous iron oxides, some iron-oxyhydroxides, and several substituted iron oxides, eg. $Ce_{1-x}Fe_xO_2$, yield a RT doublet similar to D.[9,25−27] Thus, unequivocal assignment from the RT Mössbauer parameters of the doublet D does not seem to be possible. It should also be noted that the δ and Δ values obtained for D do not show significant variation from 95Fe to 50Fe sample, indicating that the s-electron charge distribution of the Fe^{3+} ions in D species is not influenced by the Ce-content of the catalyst. Small differences in the line width of D among the three catalysts are not significant.

If the origin of D were related to the existence of finely divided phases, an spm behavior of D at low temperatures would be expected. Determination of low-temperature parameters and the temperature, or temperature-range, at which the doublet-to-sextet transition takes place can also help in the assignment of D. Thus, a series of low-temperature Mössbauer spectra were recorded from 95Fe, 85Fe, and 50Fe catalysts (Figures 8 and 9). These figures show that upon lowering the recording-temperature, a broad magnetic component gradually starts to increase in the spectrum at the expense of doublet D, which remains with a significant concentration at 13 K in 50Fe and vanishes below 65 and 13 K in the 95Fe and 85Fe spectra, respectively. In this low-

(25) Murad, E.; Johnston, J. H. Iron oxide and hydroxides. In *Mössbauer Spectroscopy Applied to Inorganic Chemistry*; Long, G. J., Ed.; Plenum Press: New York, London, 1987; Vol. 2, pp 507−582.
(26) Vandenberghe, R. E.; De Grave, E.; Landuydt, C.; Bowen, L. H. *Hyperfine Interact.* **1990**, *53*, 175.
(27) Zboril, R.; Mashlan, M.; Petridis, D. *Chem. Mater.* **2002**, *14*, 969.
(28) (a) Robbins, M.; Wertheim, G. K.; Menth, A.; Sherwood, R. C. *J. Phys. Chem. Solids* **1969**, *30*, 1823. (b) Berry, F. J.; Jobsen, S.; Jones, S. L. *Hyperfine Interact.* **1989**, *46*, 613.

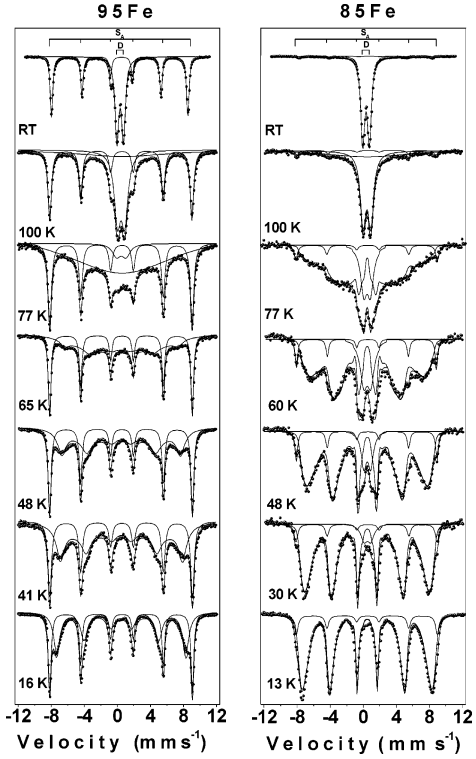

Figure 8. Mössbauer spectra recorded at low temperatures from 95Fe and 85Fe catalysts.

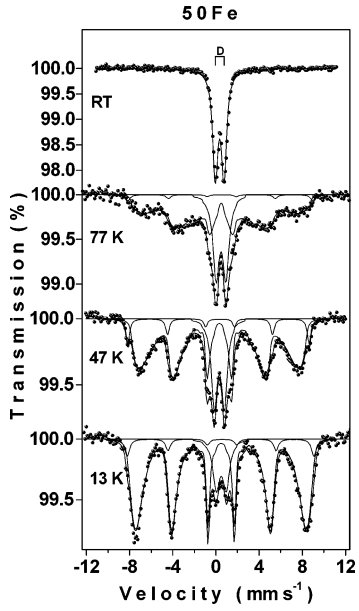

Figure 9. Mössbauer spectra recorded at low temperatures from the 50Fe catalyst.

temperature behavior, the three samples seem to follow a similar pattern: at the beginning, a large broadening is exhibited by the emergent component, after the new component has changed to a broad sextet, which becomes sharper and with a higher hyperfine magnetic field as the recording temperature decreases. The strong line-broadening, which appears in the 100−47 K range, is characteristic of magnetically ordered systems exhibiting relaxation effects close to their magnetic order temperature.[29] In contrast, a classic spm system with a particle size distribution would have shown a

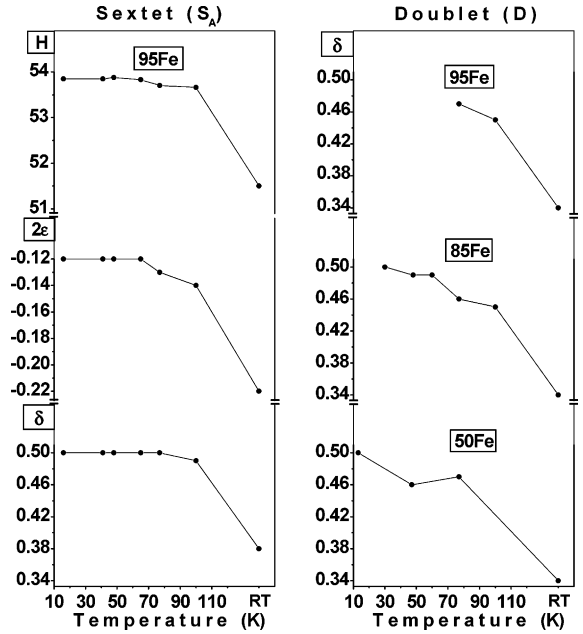

Figure 10. Mössbauer parameters at low temperatures (δ and 2ϵ in mm s^{-1} and H in Tesla). Left: Variation with temperature of δ, 2ϵ, and H of sextet S_A in the 95Fe catalyst. Right: Variation with temperature of δ of doublet D in 95Fe, 85Fe, and 50Fe catalysts.

low-temperature pattern constituted by doublet/sextet coexistence over a large temperature range, without the broad magnetic resonance accounting for paramagnetic relaxation.[29,30] Nevertheless, in 85Fe and 95Fe samples, when the broad component splits into a sextet (below 47 K, approximately), both outermost peaks of the sextet exhibit an asymmetrical line broadening, similar to that of spm-systems with a particle size distribution. Thus, in principle our series of low-temperature spectra indicate that a magnetically ordered phase exhibiting relaxation effects is present in the three catalysts and that this phase seems to display some type of spm-like behavior, especially in the 85Fe and 50Fe catalysts. Accordingly, as mentioned in the Experimental Section, low-temperature spectra were fitted by combining hyperfine magnetic field (H) distribution and single-line procedures. The fitted spectra and the most relevant parameters obtained from the fits are shown in Figures 8 and 9 and Figure 10, respectively.

The low-temperature parameters obtained for S_A (see Figure 10) from the 95Fe spectra are in reasonable agreement with the data published for hematite.[25−27] The 47 and 77 K spectra of the 50Fe and 85Fe samples show two narrow peaks at the external sides of the broad magnetic component (Figures 8 and 9). The positions of these peaks coincide with peaks 1 and 6 of the hematite. The histograms of H probabilities corresponding to the spectra mentioned (not shown) also exhibited a maximum at $H \approx 52.8$ T. This maximum indicates the presence of a six-line well-ordered phase, which must necessarily be masked by the broad magnetic component. The χ^2 of the fits improved slightly when a sextet was added to the fits (Figures 8 and 9). Despite

(29) Daniels, J. M.; Rosencwaig, A. *Can. Phys.* **1970**, *48*, 381.

(30) Vandenberghe, R. E.; De Grave, E. Mössbauer effect study of oxidic spinels. In *Mössbauer Spectroscopy Applied to Inorganic Chemistry*; Long, G. J., Grandjean, F., Eds.; Plenum Press: New York, 1989; Vol. 3, pp 59−182.

the difficulty involved in carrying out a reliable assignation of the sextet obtained, because some of its parameters had to be fixed in the fit, the results indicate that a small amount (~8%) of a phase, compatible with hematite, is also present in the 85Fe and 50Fe catalysts.

Analysis of the low-temperature data shows that in all three samples the broad resonance pattern (S_D) coming from D starts to be visible at 100 K, and both D and S_D evolves according to the expected trend of increasing isomer shift (δ) at lower temperature (see δ values obtained for *D* in Figure 10, right). The parameters obtained for S_D at each temperature do not show significant changes among the three samples, being almost coincident at 15 K ($\delta = 0.48$ mm s^{-1}, $2\epsilon = 0$ mm s^{-1}, and *H* (max. prob.) ≈ 49 T). This indicates that the same Fe species are responsible for $D-S_D$ in all three spectra. An interesting observation is that the D/S_D ratio at a given temperature was always higher in the 50Fe spectra than in the spectra of the other two samples, and it was also higher in 85Fe than in 95Fe. The above changes could be due to differences in the dilution of the magnetic interactions originated by the presence of Ce ions around the Fe^{3+} sites and/or by crystalline imperfections. If the origin of *D* is related to magnetic dilution, this would increase from the 95Fe to the 50Fe sample; that is, as the Ce-content increases. We shall discuss this issue later.

The values obtained for the quadrupole interaction of *D* in the magnetically ordered state ($2\epsilon(S_D) \cong 0$) do not correlate with those of the other magnetically ordered iron oxides or oxyhydroxides, except ferrihydrite and γ-Fe_2O_3.[25−27] According to several authors,[25,26,31] the Mössbauer spectrum of ferrihydrite recorded at 77 K contains only a single doublet with temperature-independent splitting of $\Delta = 0.62 \pm 0.04$ mm s^{-1}. Thus, the whole doublet *D* cannot be attributed to ferrihydrite because our 77 K spectra had already revealed a broad magnetic pattern coming from *D*. Additionally, the synthesis conditions, as well as the XRD data, preclude the presence of spm $\gamma-Fe_2O_3$ and ferrihydrite in the catalysts.

It is well-known that in the iron-oxides both the chemical substitution of other elements by Fe or the presence of crystalline defects may produce a weakening of the magnetic interactions in the structure, leading to a reduction of the magnetic hyperfine field and also to lowering of the magnetic order temperature.[32] In our case, it is possible that the presence of increasing amounts of Ce ions in the structure could dilute the magnetic interactions and even lead them to collapse at room temperature, giving rise to a Mössbauer spectrum constituted by a paramagnetic doublet. The RT parameters of our doublet are identical to those of the doublet reported by Li et al.[9] for the $Ce_{1-x}Fe_xO_2$ system ($x = 0.05$, 0.15). The Raman, EPR, and Mössbauer results led these authors to conclude that in that system high-spin Fe^{3+} ions are distributed at a 3:1 ratio (imposed by the stoichiometry) between the Ce^{4+} sites and the interstitial sites. It was obvious that the magnetic interactions decreased as Ce-content increased, and that the weakening of the magnetic interactions lowered the temperature of magnetic order. According to this, the different evolution of the doublet with temperature observed for the three catalysts studied here must be related to the increase in the Ce content in the sample.

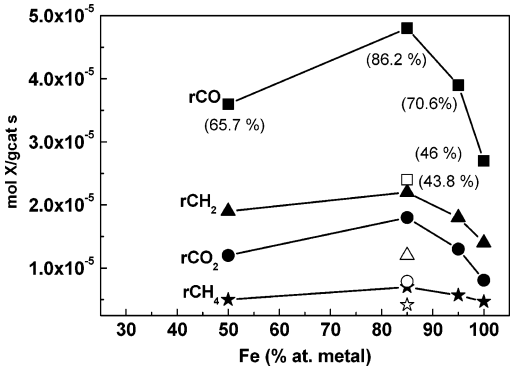

Figure 11. Catalytic activity of different catalysts at TOS = 5700 min in terms of CO conversion rate, hydrocarbon (CH_2) formation rate, CO_2 formation rate, and CH_4 formation rate. X_{CO} % are shown in brackets for each catalyst. Closed symbols correspond to coprecipitated samples and open symbols correspond to PM85Fe sample.

Finally, it was clear that the 95Fe catalyst contained an important amount of hematite (~40%), whereas only a small amount of hematite (≤8%) was found in the 85Fe and 50Fe catalysts. This is in agreement with the findings reported by Li et al.[9] that demonstrated that with increasing Fe-contents (above $x = 0.2$) a second phase of hematite was formed besides the existing $Ce_{1-x}Fe_xO_2$ solid solution.

In summary, the Mössbauer study showed that ferric species other than the hematite were present in the three Fe−Ce catalysts. These species, typical of high-spin Fe^{3+} ions occupying distorted octahedral sites, are paramagnetic at RT and magnetically split below 100 K, giving relaxation spectra. The doublet−sextet transition starts at the same temperature in all three catalysts, but doublet and relaxation spectral features remain in the spectrum over a temperature range that tends to increase in the order of the 95Fe < 85Fe < 50Fe spectra because of the different diminishing rate of doublet *D*. The doublet is still present in the 13 K spectrum of the 50Fe sample. The RT parameters of *D* coincide with those of the doublet reported for $Ce_{1-x}Fe_xO_2$.[9] Besides the ferric species *D*, low-temperature data point to the presence in the 95Fe sample of an important amount (~40%) of a large particle magnetically ordered phase, compatible with hematite, while small amounts (8%) of a phase compatible with spm-hematite seem to be present in the 85Fe and 50Fe samples.

CO Hydrogenation Activity. The catalytic properties of the different solids tested in this work changed during time on-stream (TOS). Initially, the catalysts deactivated, the rate of such deactivation depending on the type of samples. However, after a certain period of time, which differed from sample to sample, the catalysts underwent a progressive increase in activity. Figure 11 depicts the rate of CO conversion, together with the rate of formation of CO_2, of hydrocarbons (expressed as the amount of CH_2 units), and of methane over the Fe−Ce catalysts after 5700 min TOS (conversion even continued to increase and no deactivation was observed after this point, but this time was selected as

(31) Madsen, M.B.; Morup, S. *Hyperfine Interact.* **1986**, *27*, 329.
(32) Murad, E. Application of ^{57}Fe Mössbauer spectroscopy to problems in clay mineralogy and soil science: possibilities and limitations. In *Advances in Soil Science*; Stewart, B. A., Ed.; Springer-Verlag: New York, 1990; Vol. 12, pp 125−157.

Table 3. Catalytic Properties in Fischer−Tropsch Synthesis of Fe−Ce Catalysts at Isoconversion

catalyst	X_{CO} (%)	TOS (min)	Selectivity (%, C base) CO_2	C_1	C_2-C_5[a]	C_6-C_{12}[b]	C_{12+}[c]	C_{oxyg}	olefinicity[d]
100Fe	49.1	1180	29.4	21.2	55.7	16.2	1.2	5.7	35.8
95Fe	52.5	3980	32.4	25.1	55.2	14.5	0.6	4.5	43.6
85Fe	47.6	2040	33.0	23.2	55.3	16.2	0.7	4.7	46.3
50Fe	48.9	3585	31.5	20.6	51.5	21.1	1.6	5.3	45.2
PM85Fe	49.8	1515	31.6	22.0	55.5	15.6	1.5	5.4	34.1

[a] Hydrocarbons with 2−5 carbon atoms. [b] Hydrocarbons with 6−12 carbon atoms. [c] Hydrocarbons with more than 12 carbon atoms. [d] % of olefins of total amount of hydrocarbons.

the period on-stream during which catalysts are satisfactorily activated). The figure clearly shows that the addition of Ce by the coprecipitation method increases the CO conversion rate with respect to that of pure Fe. This improvement is a consequence of the improvement in all the product groups represented in Figure 11: CO_2, hydrocarbons, and methane. In the case of the PM85Fe sample, these improvements were not observed and the values were slightly below those of Fe sample. The Ce sample showed negligible activity. The 85Fe sample was found to be the most active catalyst and the values of the reaction rates were 2-fold higher than those of Fe. The 95Fe catalyst also displayed higher production rates than those of the pure Fe sample. The 50Fe coprecipitated catalyst showed slightly lower production rates than the 95Fe sample, although they were still better than those of Fe (although it should be taken into account that 50Fe must contain very active Fe sites: the intrinsic production rate for the different products expressed per g of Fe was the highest since this sample contained half the Fe concentration).

Table 3 summarizes the selectivity toward different fractions of the products group at isoconversion (to obtain the same conversion different TOS were required). Initially, the selectivities to the different hydrocarbons also underwent visible changes with TOS, but after a given time in the reaction mixture, the selectivities remained fairly constant. The values tabulated are very representative of those obtained after sufficient TOS. Ce addition by coprecipitation samples resulted in a visible increase in the olefinicity of the FT product. This effect is typical of basic additives in general. The incorporation of Ce by physical mixing did not result in any modification of the olefinicity. However, other typical consequences of rare earth additions, such as a higher water-gas shift (WGS) activity (visible in the higher CO_2 selectivity) or a higher selectivity toward liquid hydrocarbons[33] were not clearly observed. Neither were the changes introduced in the Fe catalysts by typical basic additives (K, etc)[34] observed as higher WGS activity or higher wax production.

Discussion

The characterization results obtained here showed that all the Fe−Ce coprecipitated samples displayed distinctive features that were not visible when the samples were prepared by physical mixing of the pure precursors. The disparate features can be explained in terms of the formation of mixed oxides with hematite-like or cubic ceria-like structures, depending on the relative Fe and Ce concentrations. Apparently, and according to the XRD and Raman results, the situation could be described as follows. The 95Fe sample, with only 5% of metallic atoms as Ce, could be envisaged as a mixed oxide with the hematite structure in which part of the Fe cations have been replaced by Ce^{4+}. Higher Ce concentrations (85Fe sample) would result in a very amorphous material. It seems that this concentration is in the border region that separates two different types of behavior: one in which Ce is being dissolved in the hematite structure, and the other one in which Fe is being dissolved in the ceria structure. At 15% Ce composition, no clear definite mixed oxide is formed. Actually, it appears that in the 85Fe sample both hematite and *c*-CeO_2-like solid solutions may coexist together. Although the XRD of 85Fe corresponds to a very amorphous sample, weak and very broad XRD reflections that could be assigned to hematite and to cubic ceria were visible.

Nevertheless, Mössbauer spectroscopy, a technique sensitive to the short-range surrounding of the Fe sites, throws a different light on this simplified vision. The key result that leads to a revision of the interpretation of the XRD and Raman results is the presence of the doublet signal detected in all the Fe−Ce coprecipitated samples. A clue about this comes from the fact that this signal is the only feature detected in the 50Fe sample. The XRD and Raman results revealed the presence of a *c*-CeO_2-like solid solution in which part of the Ce^{4+} cations were substituted by Fe^{3+}. Taking these findings into account, we are prompted to conclude that the ferric species visible as the *D* signal in the 50Fe sample arises from the Fe^{3+} cations dissolved in the *c*-CeO_2 structure. As explained in the Results section, Fe^{3+} cations enter the ceria framework through the interstitial substitution mechanism, which obviously affords the Fe^{3+} cations the particular coordination needed for the unique *D* signal.

Once it is accepted that the *D* signal is proof of the existence of Fe dissolved in the ceria structure, a very plausible hypothesis would be that the ceria-like solid solution would be present in the other Fe−Ce coprecipitated samples. In the case of the 85Fe sample, the Mössbauer data indicate that around 95% of the Fe is detected as the *D* doublet and therefore exists in a local environment similar to that present in the 50Fe sample: Fe dissolved in the ceria structure. The rest remains, as seen in Table 2 and from the low-temperature spectra, in the hematite-like structure. The fact that the CeO_2 features in the XRD and Raman study were not identified indicates that the Fe−Ce solid solution is very amorphous. According to Table 2, a small amount of Fe (5%) is present as hematite that must also be ill-crystallized because it was XRD- and Raman-silent as well. A similar situation is seen in the 95Fe sample. In this case, the XRD and Raman results indicate that only the hematite-like solid solution is visible. However, its Mössbauer spectrum reveals that an important fraction of the Fe cations (around 50%!) are not Raman- and XRD-detectable and lie within the framework of an ill-crystallized ceria-like

(33) Wang, D.; Cheng, X.; Huang, Z.; Wang, X.; Peng, S. *Appl. Catal.* **1991**, *77*, 109.
(34) Nganstsoue-Hoc, W.; Zhang, Y.; O'Brien, R. J.; Luo, M.; Davis, B. H *Appl. Catal. A: Gen.* **2002**, *236*, 77.

solid solution as well. The rest of the Mössbauer signal arises from the hematite sextet, the phase detected by XRD and Raman.

It is very remarkable that the CeO_2-like structure can dissolve such a high amount of Fe^{3+}. In the case of 95Fe sample, a rough estimation indicates that only 10% of the metallic cations in the ceria-like solid solution are Ce cations. The rest are Fe^{3+} cations (90%!). It has been pointed out that the CeO_2 system is very flexible (a large fraction of the positions available for cations are not occupied) and can admit strong Ce substitution by other different sized metallic cations.[13] For instance, it is well-known that CeO_2 can hold up to ca. 80−90% of metal cations as Zr^{4+}. In this case, the cubic ceria structure is distorted and although Ce cations still keep their fluorite-like environment Zr coordination shell is modified in such a way that the material adopts tetragonal symmetry.[13] In the latter case, neither the vacancy compensation mechanism nor the interstitial substitution mechanism are needed for isovalent Zr^{4+} substitution. The aliovalent Fe^{3+} and the special rearrangement needed to accommodate Fe^{3+} in the ceria framework (interstitial mechanism) seems to result in very deep distortion and a poor crystallization of the initially cubic ceria. In the 50Fe system, the structure is crystalline but the similar Mössbauer parameters of the Fe^{3+} in the 95Fe, 85Fe, and 50Fe samples indicate that the short-range order around iron is alike in all of them and hence the basic architecture of the structure is maintained in the ceria-like solid solution. In contrast, the hematite structure is not so flexible, and only a small amount of such a large cation (Ce^{4+}) is expected without instability of the crystalline structure. The low substitution of the hematite-like solid solution would explain that the Mössbauer parameters are very similar to those of the pure hematite.

Finally, it is worth stressing that Mössbauer spectrosocopy also reveals that calcination at high temperatures drives the segregation of pure phases from the mixed oxides. The sextet of hematite dominates the spectrum of 50Fec973, see Figure 7 and Table 2, although a weaker contribution from the doublet arising from the Fe dissolved in CeO_2 structure still remains in it.

In summary, it can be said that the coprecipitation procedure leads to the formation of solid solutions in which Fe or Ce are dissolved within a ceria or hematite structure, respectively. Moreover, the coprecipitation method is required for the formation of the mixed oxides and the physical mixture (and physical mixing) of the precursors fails. The coprecipitation method is an accepted methodology when mixed metal oxides are to be prepared. The cations are expected to be in intimate contact, or at least in closer contact, in the precursors thus formed. This obviously facilitates the solid-state reactions that result in the formation of mixed oxides when the precursor is decomposed by calcination at high temperature.[35] In the Fe−Ce samples, this close contact could not be accomplished by physical mixing. Even calcination at higher temperature of the physical mixtures for the solid-state reaction to develop mixed oxides should fail because in this case segregation of the pure Fe and Ce oxides takes place instead.

One of the most remarkable consequences of the formation of mixed oxides is that a direct Fe−Ce interaction appears. This interaction, achieved only by coprecipitation, takes place through the sharing of O anions defined by the Fe−O−Ce bonds formed either in the hematite-like mixed oxide or in the *c*-CeO_2-like mixed oxide.

Another consequence of the formation of the mixed oxide is the increase in specific surface area with respect to the pure Fe or Ce sample (pure α-Fe_2O_3 and *c*-CeO_2). This rise is more remarkable in the low Ce concentration region. To explain this increase, it must be taken into account that the coprecipitated solids comprise two kinds of phases: hematite-like and ceria-like solid solutions. The enlargement of the specific surface area of hematite derived from ferrihydrite prepared by the coprecipitation of Fe^{3+} with other cations such as M = Si^{4+}, Al^{3+}, and Mo^{6+} has been reported previously. The reason is that the growth of ferrihydrite crystallites that occurs during calcination to yield hematite is prevented because part of these cations present during the precipitation of Fe^{3+} remain adsorbed on the surface of ferrihydrite crystallites.[36−38] It has been shown that coordinately unsaturated sites (CUS) are present at the surface of the ferrihydrite crystals. If no other element is present, water from the solution is adsorbed on the CUS. When the ferrihydrite decomposes under calcination, these water molecules are released from the particle interface, leading to the condensation of the eventually formed Fe oxihydroxide crystals, with the subsequent agglomeration and the formation of larger α-Fe_2O_3 particles at the end. When cations such as Si^{4+}, Al^{3+}, and Mo^{6+} are present in the coprecipitating solution, some of them can be chemisorbed on the CUS and form Fe−O−Me complexes at the ferrihydrite surface (the rest are trapped within the Fe oxihydroxide structure because of the coprecipitation). During the formation of α-Fe_2O_3 by calcination, these cations cannot be released to the gas phase, as water molecules are, which prevents the agglomeration of the small Fe oxihydroxide crystals. The final result is that the α-Fe_2O_3 thus formed displays a higher specific surface area because of the smaller crystal size.[36−38]

This might be well the case of the hematite-like Fe−Ce solid solution described in this article. Some of the Ce^{4+} cations present in the solution end up adsorbed on the ferrihydrite CUS sites formed during the coprecipitation process (even though the Ce salt used for the preparation is Ce^{3+} nitrate, this cation is expected to be rapidly oxidized to Ce^{4+} at basic pH). It must be borne in mind that when the drops of the metallic solutions become dissolved in the precipitating solution, during the first moments of contact between the drops and the basic solution, local spots with an acid pH still remain. Therefore, it is very likely that during these very early moments some Fe^{3+} will precipitate as small ferrihydrite crystals. Then, some of the Ce^{4+} cations can be

(35) Schüth, F.; Unger, K. In *Handbook of Heterogeneous Catalysis, Vol. 2: Preparation of Solid Catalysts*; Ertl, G., Knözinger, H., Weitkamp, J., Eds.; Wiley-VCH: Weinheim, Germany, 1999; pp 60−98.

(36) Zhao, J.; Fheng, Z.; Huggins, F. E.; Shah, N.; Huffmann, G. P.; Wender, I. *J. Catal.* **1994**, *148*, 194.

(37) Zhao, J.; Fheng, Z.; Huggins, F. E.; Shah, N.; Lu, F.; Huffmann, G. P. *J. Catal.* **1993**, *143*, 499.

(38) Zhao, J.; Fheng, Z.; Huggins, F. E.; Huffmann, G. P. *Energy Fuels* **1994**, *8*, 38.

adsorbed on the CUS sites of the ferrihydrite crystals. During calcination, these adsorbed Ce^{4+} cations prevent the formation of larger Fe oxide particles. Moreover, the Fe−O−Ce complexes thus formed at the surface of the ferrihydrite crystals may be the precursors of the formation of the hematite-like Fe−Ce solid solution during the calcination step.

Concerning the *c*-CeO_2-like solid solution another explanation could be offered to account for the high specific surface area. In this case, the mixed oxide adopts the *c*-CeO_2 structure. Some trivalent cations such as Al^{3+}, La^{3+}, Nd^{3+}, and Y^{3+} forming solid solutions with a CeO_2 structure stabilize them against thermal sintering.[39] This effect has been explained in terms of the inhibition of the sintering rate-limiting step, the surface diffusion of cerium defects, caused by the presence of trivalent cations at the surface of CeO_2.[40]

Regarding the properties of the catalysts derived from the Fe−Ce systems investigated in this work, the most remarkable conclusion is that catalysts prepared by coprecipitation display better catalytic conversion than those prepared by physical mixing. In other words, catalysts in which an Fe−O−Ce interaction is developed in the oxide form exhibit better catalytic properties. Achieving the final state of FT catalysts based on Fe requires in-situ activation of the calcined sample under the reaction conditions. This process leads to a rearrangement of the bulk and of the surface of the catalyst, resulting in the formation of new phases that are very different from those found in the calcined sample (that loaded in the catalytic reactor). It is widely accepted that the Fe phases undergo a reduction process that, in the reaction mixture (H_2+CO atmosphere), results in the (partial) carburization of the Fe phases: several Fe carbides have been reported to be formed under the reaction conditions.[41] Indeed, it has been proposed that the active phase for the FT process is an Fe carbide-like site.[42] The exact nature (physical and/or chemical appearance) of the Fe−Ce interaction in the final coprecipitated catalyst can no longer be described by the Fe−O−Ce bridges formed in the solid solutions. However, regardless of the actual state of the catalyst after 5700 min TOS, it is clear that it is determined by the initial Fe−O−Ce interaction developed in the oxide state and that it is different from the catalytic nature of the pure Fe sample and of the PM samples in which this Fe−O−Ce interaction is not developed.

It can be speculated that the effects observed for the Ce-promoted catalysts can be rationalized in terms of the two mechanisms proposed to explain promotion by basic additives: chemical and structural promotion. The chemical promotion by alkali additives is still a matter of debate and is complicated by the fact that many variables (method of preparation, temperature of calcination, temperature of reduction, operation conditions, etc.) affect the final result.[43−45] However, it is proposed that the electropositive character of the alkali additives would involve an increase in the electronic density of the Fe site. In general it is admitted that the alkali promoter results in measurable changes of the thermodynamic and kinetic properties of the adsorption of CO and H_2[46,47] affecting their relative surface coverages and reactivity. Under the most favorable circumstances, the electropositive promoter will enhance the CO/H_2 ratio at the surface. Moreover, the promotion also increases the dissociation rate of the C−O bond. The final situation is a lower H/C ratio at the surface that eventually leads to the hydrogen-poor product mixture (higher olefinic character) and higher catalytic activity. In our case, it is proposed that in all the coprecipitated catalysts a close Fe−Ce interaction in the final catalyst would result in a direct effect for Ce ions in the direction explained above for other basic promoters. In the case of Fe−Ce catalysts prepared from physical mixtures, the Fe−Ce interaction does not seem to develop, and therefore olefin selectivity should be the same as that of the 100Fe catalyst.

Nevertheless, it is also well accepted that a depletion of the availability of surface hydrogen by basic additives also causes the formation of the heaviest products and the lowest methane formation. Such effects were not observed in the coprecipitated samples studied here. This draws attention to structural promotion: the formation of the solid solutions enables the formation and stabilization of small particles of mixed oxides and, when activated in reaction mixtures, the catalyst can still maintain a high specific area. This results in material with a larger number of exposed active sites and with higher catalytic activity. The participation of this structural promotion cannot be discarded. In fact, the volcano-like curve of the catalytic activity strongly resembles that of the specific surface of the oxide precursors.

Acknowledgment. The European Commission is gratefully acknowledged for funding Project ENKT6-CT-2002-00682 under the 5th Framework Program. The Spanish Ministry of Science and Technology is also acknowledged for funding the MAT2001-2215-C03-01 project. F.P. also thanks the Spanish Ministry of Science and Technology for a doctoral fellowship.

CM0477669

(39) Kašpar, J.; Fornasiero, P.; Graziani, M. *Catal. Today* **1999**, *50*, 285.
(40) Pijolat, M.; Prin, M.; Soustelle, M.; Touret, O.; Nortier, P. *Solid State Ionics* **1993**, *63−65*, 785.
(41) Van der Laan, G. P.; Beenackers, A. A. C. M. *Catal. Rev.-Sci. Eng.* **1999**, *41*, 255.
(42) Riedel, T.; Shultz, H.; Scahub, G.; Jun, K.-W.; Hwang, J.-S.; Lee, K.-W. *Topics Catal.* **2003**, *26*, 41.
(43) Rankin, J. L.; Bartholomew, C. H. *J. Catal.* **1986**, *100*, 526.
(44) Bartholomew, C. H. In *New Trends in CO Activation*; Guczi, L., Ed.; Studies in Surface Science and Catalysis Series; Elsevier Science Publishers: Amsterdam, The Netherlands, 1991; Vol. 64, p 159.
(45) Ehason, S. H.; Bartholomew, C. H. *Appl. Catal. A: Gen.* **1999**, *186*, 229.
(46) Kiskinova, M. In *New Trends in CO Activation*; Guczi, L., Ed.; Studies in Surface Science and Catalysis Series; Elsevier Science Publishers: Amsterdam, The Netherlands, 1991; Vol. 64, p 37.
(47) Rodriguez, J. A.; Goodman, D. W. In *New Trends in CO Activation*; Guczi, L., Ed.; Studies in Surface Science and Catalysis Series; Elsevier Science Publishers: Amsterdam, The Netherlands, 1991; Vol. 64, p 87.